KYBERNETIKA — VOLUME 35 (1999), NUMBER 1, PAGES 69 - 81

H_∞ CONTROL DESIGN FOR AN ADAPTIVE OPTICS SYSTEM

NIKOLAOS DENIS, DOUGLAS LOOZE, JIM HUANG AND DAVID CASTAÑON

In this paper we first present a full order H_∞ controller for a multi-input, multi-output (MIMO) adaptive optics system. We apply model reduction techniques to the full order H_∞ controller and demonstrate that the closed-loop (CL) system with the reduced order H_∞ controller achieves the same high level of performance. Upon closer examination of the structure of the reduced order H_∞ controller it is found that the dynamical behavior of the reduced order H_∞ controller can be accurately approximated by a single-input, single-output (SISO) transfer function (TF) multiplied by the inverse of the adaptive optics plant dc gain. This observation then leads to a general design methodology which only requires the synthesis of a SISO H_∞ controller and multiplication by constant matrices.

1. INTRODUCTION

The needs for high-resolution imaging of objects in space and efficient transmission of laser energy through the atmosphere have motivated the development and use of adaptive optics [2], [10] - [11]. Adaptive optics systems improve the performance of optical systems by reducing the effects of atmospheric turbulence. An adaptive optics system uses a measured (ideally flat) reference wavefront to estimate the aberration induced by the turbulence, and to adjust the shape of a deformable mirror to remove the aberration using CL feedback control. A growing number of applications of adaptive optics demonstrate that the feedback control approach is effective [3, 5].

Most feedback systems for adaptive optics have used integral feedback of the measured wavefront error above each actuator to control that actuator [1, 4]. This simple, local feedback design approach works provided two assumptions are satisfied: the influence function of the deformable mirror is nearly diagonal; and the bandwidth of the CL system is significantly less than the dynamics of the mirror and the limitations imposed by measurement and processing delays in the adaptive optics system. However, increasing demands on the performance of adaptive optics systems require bandwidth increases to the point that these assumptions may not hold. More sophisticated control system design and analysis techniques can achieve the desired performance by accounting for the coupling introduced by the influence functions and the relevant dynamics of the measurement delays.

In this paper we first present a full order H_∞ controller for the adaptive optics system. The H_∞ controller is designed for a MIMO adaptive optics plant model augmented by weighting functions that specify the CL frequency domain performance characteristics. The H_∞ controller has the same order as the augmented adaptive optics plant, which makes it more complex than the traditional PID-based adaptive optics controllers. We apply model reduction techniques to the full order H_∞ controller and demonstrate that the CL system with the reduced order H_∞ controller achieves the same high level of performance. Upon closer examination of the structure of the reduced order H_∞ controller it is found that the dynamical behavior of the reduced order H_∞ controller can be accurately approximated by a SISO TF multiplied by the inverse of the adaptive optics plant dc gain. This observation then leads to a general design methodology which only requires the synthesis of a SISO H_∞ controller and multiplication by constant matrices.

2. PLANT DESCRIPTION

The relevant components of the experimental adaptive optics system at Adaptive Optics Associates (AOA) consists of a 16 actuator deformable mirror, a wavefront sensor operating at 1 KHz, a wavefront reconstructor, power amplifiers, and the feedback compensator. The 16 actuators are arranged in a 4×4 square grid. Figure 1 presents the block diagram of the adaptive optics system used for the control design.

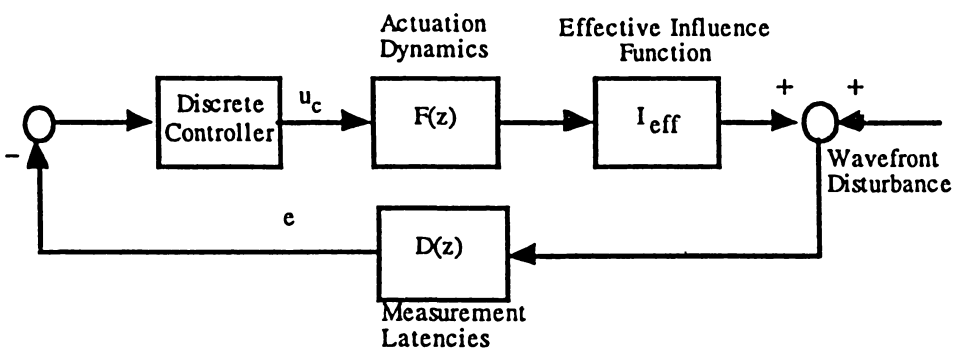

Fig. 1. The adaptive optics system.

In Figure 1, the effective influence function is a static linear map (matrix) which takes as its input the 16 mirror drive voltages and produces the shape of the deformable mirror over the 16 actuator positions, as seen through the wavefront sensor/wavefront reconstructor pair. It is a highly coupled matrix for three reasons. First, there is spillover of the influence function from one actuator to its neighboring actuators. We have experimentally determined that this amounts to approximately 10 % coupling between linearly adjacent actuators, and 7 % coupling between diagonally adjacent actuators. Second, the wavefront sensor used in our system measures the local gradient of the wavefront over a subaperture of the mirror (a subaperture

is defined as the square region surrounded by four corner actuators). The particular way in which the local gradients are measured implies the existence of two unobservable modes: the *piston* mode, which corresponds to a constant bias term across the entire mirror; and the *waffle* mode, which resembles a breakfast waffle (equal magnitude alternating variations of the wavefront over the mirror actuator locations). Because the wavefront reconstructor is the Moore–Penrose pseudo-inverse of the wavefront sensor matrix rather than the true inverse, the wavefront reconstructor/wavefront sensor combination does not yield the identity matrix. Finally, global tip and tilt modes are typically controlled by special tip/tilt mirrors in the adaptive optics system, to avoid exceeding the dynamic range of the mirror. In the AOA system a projection matrix is included as part of the wavefront reconstructor to remove global tip and tilt modes. For these reasons, the effective influence function matrix is a highly coupled matrix. The identified influence function is presented in [7].

The dynamic system $D(z)$ corresponds to delays associated with the wavefront sensing and the reconstruction. It is a 16×16 diagonal TF matrix whose elements have the form:

$$D_{ii}(z) = \frac{1}{(1-\alpha_i)} \frac{z-\alpha_i}{z^{l_i}} \quad \text{for } i = 1, \ldots, 16. \tag{1}$$

The dynamic system $F(z)$ corresponds to dynamics associated with the power amplifiers and the piezo-electric actuators pushing the mirror. It is also a 16×16 diagonal TF matrix whose elements have the form:

$$F_{ii}(z) = \frac{(1-\beta_i)}{(z-\beta_i)} \quad \text{for } i = 1, \ldots, 16. \tag{2}$$

Note that the elements of $D(z)$ and $F(z)$ have been normalized to have unit magnitude at $z = 1$. Any nonunity gain has been attributed to the effective influence function matrix. The identified values for α_i, β_i and l_i can be found in [7].

3. PERFORMANCE SPECIFICATIONS

The controllers are to achieve 100 Hz bandwidth on the CL TF matrix. We will also obtain near -6 dB disturbance rejection at 30 Hz, which is a typical Greenwood frequency (characteristic frequency of the atmosphere [10]) for adaptive optics systems. In addition, we will require that the peaks at the natural frequency of the CL system to be less than 15 dB to obtain good transient characteristics. Note that all of the above performance specifications apply to the singular values of the corresponding TF matrices evaluated at the specified frequencies. There are several factors that will limit the achievable performance of the CL system. First, the wavefront sensor operates at 1000 Hz, while the general rule of thumb is to have at least a 10 : 1 ratio between the sampling frequency and the CL bandwidth. Second, the amplifier circuit $F(z)$ and the generalized latencies $D(z)$ both contribute phase lags into the system, so a simple integral control law, which appears frequently in the adaptive optics literature, may not be satisfactory. Finally, the identified plant model may contain model uncertainties, which may hinder actual performance.

4. FULL ORDER H_∞ CONTROL DESIGN

One of the recent advances in control system design is the H_∞ optimal control methodology [6]. The adaptive optics plant is a MIMO plant because it has multiple actuators which provide the plant's input signals, while the measurement signals are obtained from multiple subapertures of the deformable mirror. As mentioned above, it is a highly coupled plant and moreover there is some plant uncertainty due to noise in the influence function measurement and the unknown delays that exist between the voltage input and the OPD output. This uncertainty imposes robustness requirements on the controlled system. For these reasons, the framework of this application is well suited for an H_∞ control design.

In translating this problem into the H_∞ framework, a plant, which includes the identified adaptive optics system components as well as weighting functions, must be defined. The weighting functions serve to shape the frequency response of the CL system. Figure 2 presents the plant used in the adaptive optics H_∞ control design.

In Figure 2 $\boldsymbol{G}_{\text{eff}}(z)$ is the plant to be controlled by the control system. It consists of the deformable mirror influence function matrix and the TF matrices representing amplifier dynamics and measurement delays.

$$\boldsymbol{G}_{\text{eff}}(z) = \boldsymbol{D}_d(z)\, \boldsymbol{F}_{\text{eff}}\, \boldsymbol{A}(z). \tag{3}$$

Also in Figure 2, $\boldsymbol{K}(z)$ is the H_∞ controller to be designed, and $\boldsymbol{W}_e(z)$ and $\boldsymbol{W}_u(z)$ are weighting functions used to shape the frequency response of the CL system.

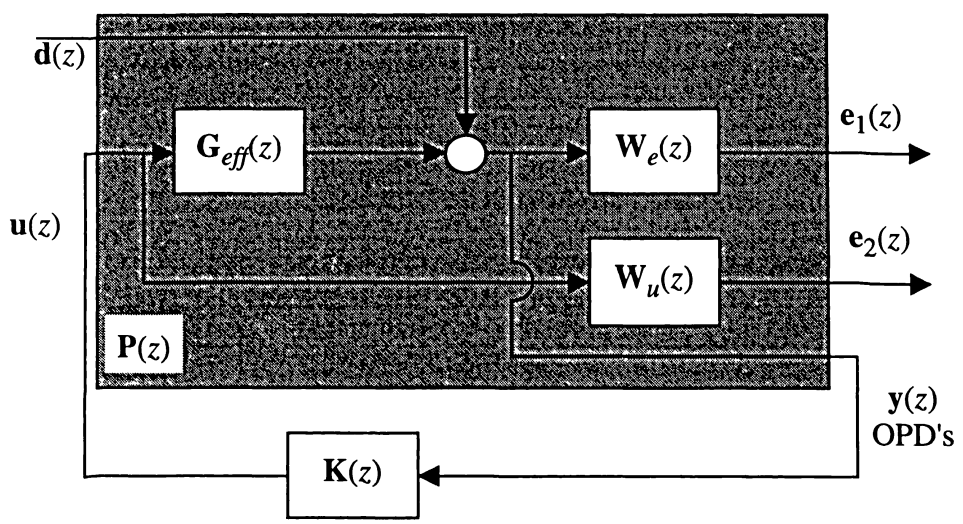

Fig. 2. Plant model used for H_∞ control design.

The plant inputs are the voltages $\boldsymbol{u}$ applied to the piezoelectric actuators, and the phase variation $\boldsymbol{d}$ induced by atmospheric aberrations of the incoming wavefront. The plant output $\boldsymbol{y}$ is a vector of the OPD's of the reflected wavefront, which

is modeled as the sum of $\boldsymbol{d}$ and the phase variation induced by the deformed mirror surface. The signals $\boldsymbol{y}$ and $\boldsymbol{u}$ are filtered by $\boldsymbol{W}_e(z)$ and $\boldsymbol{W}_u(z)$ to produce the signals $\boldsymbol{e}_1$ and $\boldsymbol{e}_2$, which serve to quantify the performance of the CL system. The poles of the augmented plant presented in Figure 2 are stable, except of the poles at $z = 1$ introduced by $\boldsymbol{W}_e(z)$. However, since these poles are controllable and observable the augmented plant satisfies the detectability and stabilizability conditions required to solve the H_∞ control problem. Furthermore, since there is full rank direct feedthrough from $\boldsymbol{d}$ to $\boldsymbol{y}$ and from $\boldsymbol{u}$ to $\boldsymbol{e}_2$, the full rank conditions are met as well. Therefore, a stabilizing H_∞ controller can be found.

The CL TF matrix $\boldsymbol{G}(z)$ maps input $\boldsymbol{d}(z)$ to the output $\boldsymbol{e}(z)$ as follows:

$$\boldsymbol{e}(z) = \begin{bmatrix} \boldsymbol{W}_e(z)(\boldsymbol{I} + \boldsymbol{G}_{\text{eff}}(z)\boldsymbol{K}(z))^{-1} \\ -\boldsymbol{W}_u(z)\boldsymbol{K}(z)(\boldsymbol{I} + \boldsymbol{G}_{\text{eff}}(z)\boldsymbol{K}(z))^{-1} \end{bmatrix} \boldsymbol{d}(z). \tag{4}$$

The weighting function $\boldsymbol{W}_e(z)$ is chosen so that:

$$\boldsymbol{W}_e(z) = \boldsymbol{W}(z)\ \boldsymbol{W}_p \tag{5}$$

where $\boldsymbol{W}_p$ takes out the piston, waffle, tip and tilt components in the measurement vector $\boldsymbol{y}(z)$ so that they are not penalized, and $\boldsymbol{W}(z)$ is chosen to be a diagonal matrix so that the projected OPD values are penalized equally.

$$\boldsymbol{W}(z) = \frac{200 \cdot T_s}{2} \frac{z+1}{z-1} \boldsymbol{I}. \tag{6}$$

In (6) T_s is the sampling rate (0.001 sec).

A weighting function $\boldsymbol{W}_u(z)$ on the signal $\boldsymbol{e}_2$ is included to penalize the CL TF from $\boldsymbol{d}$ to $\boldsymbol{e}_2$. $\boldsymbol{W}_u(z)$ was selected as:

$$\boldsymbol{W}_u(z) = 0.5 \cdot \boldsymbol{I} \tag{7}$$

where $\boldsymbol{I}$ is the identity matrix of appropriate dimensions. The purpose of this weighting was to enforce an upper bound on the CL complementary sensitivity function.

The smallest γ achieved for $\|\boldsymbol{G}(z)\|_\infty$ was $\gamma = 0.563$. In Figure 3 the SV Bode plot of the sensitivity TF matrix $\boldsymbol{S}(z)$ with input $\boldsymbol{d}(z)$ and output $\boldsymbol{y}(z)$ is presented. Four of the singular values of $\boldsymbol{S}(z)$ have a constant magnitude of 0 dB for all frequencies. These singular values correspond to the fact that the CL TF from $\boldsymbol{d}(z)$ to $\boldsymbol{y}(z)$ does not affect the piston, waffle, tip and tilt modes as desired. The disturbance rejection

bandwidth with this controller is 80 Hz.

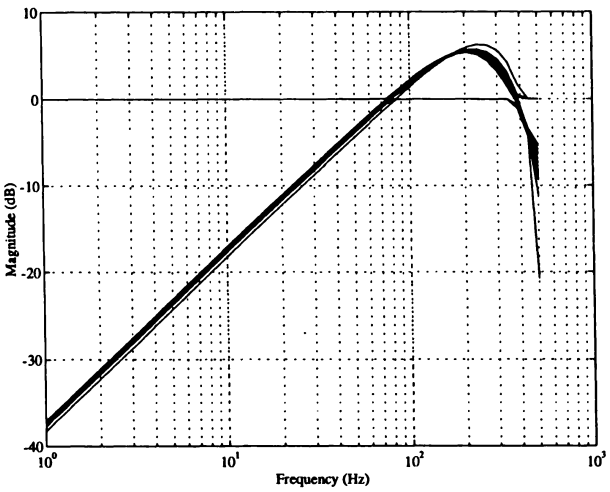

Fig. 3. SV Bode plot of $S(z)$.

In Figure 4 the singular value Bode plot of the complementary sensitivity TF, $T(z)$ matrix is presented, from which we see that the CL bandwidth of the system is 180 Hz. In Figure 4 only twelve singular values are plotted since four have zero magnitude for all frequencies. These zero singular values correspond to the fact that the CL TF from $d(z)$ to the plant output rejects the piston, waffle, tip and tilt modes as desired.

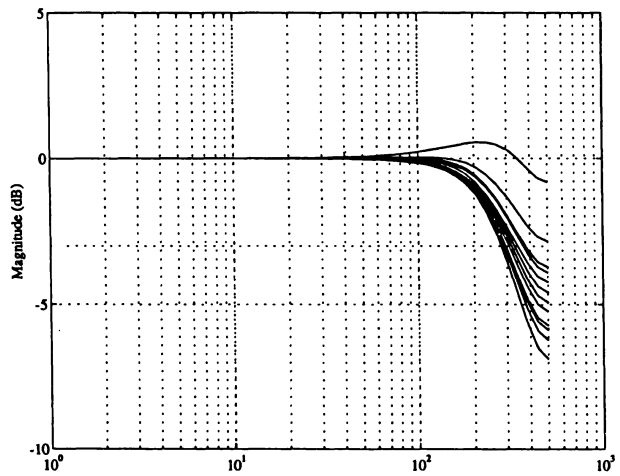

Fig. 4. SV Bode plot of $T(z)$.

5. REDUCED ORDER (24^{th}) H_∞ CONTROLLER

The H_∞ controller has the same order as the plant (plus the order of any weighting function) it attempts to control. In this case, $\boldsymbol{G}_{\text{eff}}(z)$ has 44 states and the weighting function $\boldsymbol{W}_e(z)$ has 12 states, for a total order of 56. Therefore, the H_∞ controller is a 56^{th} order controller.

It is desired to reduce the controller complexity while retaining the performance achievable by the high order H_∞ controller. This can be achieved by applying model reduction to the full order controller. A well known model reduction technique is based on balanced realization, where the state is transformed to make the controllability and observability grammians equal and diagonal, with the diagonal elements arranged in descending order. The smallest diagonal elements (Hankel singular values) represent modes that are the least controllable or observable. The parts of the state space matrices corresponding to these modes are then removed.

The Hankel singular values are invariant under similarity transformations of the state space [9]. They represent the magnitude of controllability and observability of the different modes of the system.

The 56^{th} order H_∞ controller has 39 non-zero Hankel singular values with magnitudes that vary from $2.232e+04$ to $3.287e-08$, corresponding to the controllable and observable modes of the 56^{th} order controller. Only 24 of these singular values have substantial magnitude values and thus the 56^{th} order controller was reduced to a 24^{th} order controller.

The resulting controller, when interconnected with the adaptive optics plant model, produced sensitivity and complementary sensitivity TF matrices similar to the ones produced by the full order H_∞ controller. The SV Bode plot of the sensitivity TF is presented in Figure 5.

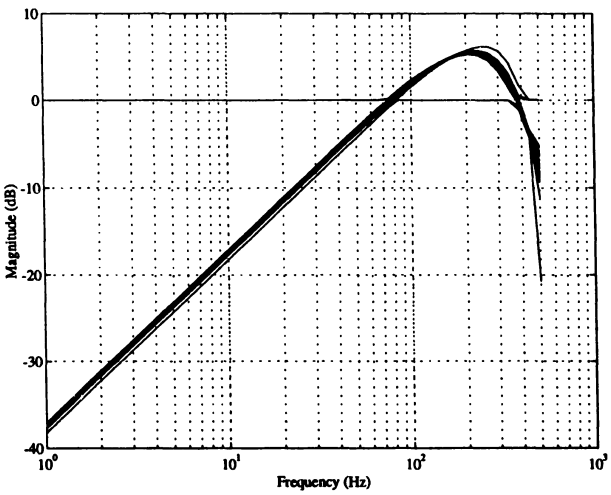

Fig. 5. Sensitivity TF with 24^{th} order H_∞ controller.

The reduced order H_∞ controller has nearly the same performance as the full

order H_∞ controller. However, by reducing the H_∞ controllers order further, the CL performance deteriorates very quickly. To illustrate this fact, the 56^{th} order controller was reduced to a 16^{th} order controller. The resulting controller, when interconnected with the adaptive optics plant, lead to an unstable CL system.

6. APPROXIMATION OF THE 24^{th} ORDER H_∞ CONTROLLER

The performance plots presented in the previous section suggests that a reduced (24^{th}) order, MIMO controller can achieve CL performance that is comparable to the full (56^{th}) order H_∞ controller.

It is noted that twelve of the poles of the 24^{th} order H_∞ controller are located at $z = 1$, while the remaining twelve controller poles vary between -0.948 and -0.509. On the other hand, all 24 zeros of the H_∞ are located near the origin. Also, the spacing between the singular values of the 24^{th} order H_∞ controller remains constant with respect to frequency. Therefore, it is postulated that the reduced order H_∞ controller can be represented by a SISO TF postmultiplied by a constant matrix. Moreover, it is further postulated that the TF has the form:

$$\alpha(z) = g\,\frac{z^2}{(z-1)(z-p)} \tag{8}$$

where the constant factor p will be selected to have a value between -0.948 and -0.598.

The method of residue estimation will be performed in order to find the constant matrix that postmultiplies $a(z)$. The constant p was set to -0.713, the average value of the reduced order H_∞ controller poles located between -0.948 and -0.5984.

6.1. Residue estimation

The method of residuals will be now used to find a 24^{th} order controller which is capable of producing the same performance as the reduced order H_∞ controller. The key is to find an approximation $\boldsymbol{K}_r(z)$ to the restriction of the reduced order H_∞ controller to V, the orthogonal complement to the subspace spanned by the piston, waffle, tip, and tilt modes. The restriction of $\boldsymbol{K}_r(z)$ to V is evaluated by using a 12×16 matrix $\boldsymbol{P}_r$ and its transpose. The latter term will be denoted by $\overline{\boldsymbol{K}}_\infty(z)$:

$$\overline{\boldsymbol{K}}_\infty(z) = \boldsymbol{P}_r \boldsymbol{K}_\infty(z) \boldsymbol{P}_r^T. \tag{9}$$

It is moreover postulated that $\overline{\boldsymbol{K}}_\infty(z)$ can be approximated by the 12×12 TF matrix:

$$\overline{\boldsymbol{K}}_\infty(z) \approx \boldsymbol{K}_r(z) = a(z)\overline{\boldsymbol{K}}_r = g\frac{z^2}{(z-1)(z-p)}\overline{\boldsymbol{K}}_r \tag{10}$$

where $\overline{\boldsymbol{K}}_r$ is a constant 12×12 matrix. An estimate $\widehat{\overline{\boldsymbol{K}}}_r$ of $\overline{\boldsymbol{K}}_r$ has to be computed such that:

$$\boldsymbol{K}_r(z) \approx g\frac{z^2}{(z-1)(z-p)}\widehat{\overline{\boldsymbol{K}}}_r. \tag{11}$$

Since $\overline{K}_\infty(z)$ has 12 poles located at $z = 1$, and $a(z)$ has a pole at $z = 1$, the residue at $z = 1$ will be evaluated on both sides of equation (10):

$$\operatorname*{Res}_{z=1}\left\{\overline{K}_\infty(z)\right\} \approx \operatorname*{Res}_{z=1}\left\{g\frac{z^2}{(z-1)(z-p)}\widehat{K}_r\right\} \tag{12}$$

which reduces to:

$$\widehat{K}_r \approx \frac{(1-p)}{g}\operatorname*{Res}_{z=1}\left\{\overline{K}_\infty(z)\right\}. \tag{13}$$

The resulting 12×12 controller is then:

$$K_r(z) = a(z)\widehat{K}_r. \tag{14}$$

Note that the constant factor g is not needed for the computation of $K_r(z)$. To make $K_r(z)$ into a 16×16 TF matrix, the matrix P_r is used again to compute $\overline{K}_r(z)$ as follows:

$$\overline{K}_r(z) = P_r^T K_r(z) P_r \tag{15}$$

$\overline{K}_r(z)$ is the desired residue controller.

To compare the performance of the controller obtained by the residue estimation to the 24^{th} order H_∞ controller, the SV Bode plots of the sensitivity and complementary sensitivity were produced and were found to be very similar to the SV Bode plots of the 24^{th} order H_∞ controller.

It is now postulated that the residue controller $K_r(z)$ is an approximate plant inverse $\widehat{K}_r$ followed by a loop shaping filter $a(z)$. To verify this, U is defined to be the four dimensional subspace spanned by the piston, waffle, tip, and tilt modes, and V to be the orthogonal complement of U, so that $\Re^{16} = U \oplus V$. Thus $\widehat{K}_r$ is compared to the restriction of the plant model at zero-frequency to V, using the 12×16 matrix P_r and its transpose. Therefore, define:

$$K_{dc} = P_r * G_{\text{eff}}(1) * P_r^T. \tag{16}$$

The constant term g was set equal to 0.7974 which minimizes the normalized error between $\widehat{K}_r$ and K_{dc}^{-1} defined as $\widehat{K}_r K_{dc} - I$. The maximum normalized error between $\widehat{K}_r$ and K_{dc}^{-1} is 4.6 %. This result suggests that the assumption previously made, that $\widehat{K}_r$ is an approximate plant inverse, is valid.

7. APPROXIMATE H_∞ CONTROL DESIGN

In Section 6 it was shown that the dynamic behavior of the 24^{th} order H_∞ controller can be accurately approximated by a SISO TF multiplied by certain constant matrices. By the method of the residue approximation, a constant 16×16 matrix, $\widehat{K}_r$, was found. This constant matrix approximates the inverse of the adaptive optics plant dc gain, when both matrices are projected to the $\Re^{12}$ space (orthogonal to piston, waffle, tip and tilt). This result suggests that the H_∞ controller attempts to diagonalize the adaptive optics plant. It is now postulated that the H_∞ controller

attempts to invert the effective influence function. However, since the effective influence function is not invertible in the $\Re^{16}$ space, it has to be projected into the $\Re^{12}$ subspace orthogonal to piston, waffle, tip and tilt, and then inverted. Once this has been achieved, diagonal compensation can be applied to the plant to obtain the required CL performance specifications.

In this section, an H_∞ controller will be designed based on a SISO model of the adaptive optics plant. The weighting matrices used during the design procedure will be the same as the ones used for the MIMO H_∞ design.

The equation used for the SISO plant is:

$$g_{\text{eff}}(z) = 100 \cdot \frac{(1-b)}{(1-a)} \frac{(z-a)}{z^2(z-b)}. \tag{17}$$

The scalar terms a and b are set to the averages of the pole and zero values used to model the amplifier and effective latency dynamics respectively. It should be noted that a SISO model for the effective influence function is not realizable and therefore it is not included in $g_{\text{eff}}(z)$.

The weighting TF $w_u(z)$ was set to 0.5 as before, while $w_e(z)$ was set equal to the diagonal element of $\boldsymbol{W}(z)$ in equation (6). Using this augmented plant configuration the close-loop system, $g(z)$, becomes:

$$e(z) = \begin{bmatrix} w_e(z)\left(\boldsymbol{I} + g_{\text{eff}}(z)\,k(z)\right)^{-1} \\ -w_u(z)\,k(z)\left(\boldsymbol{I} + g_{\text{eff}}(z)\,k(z)\right)^{-1} \end{bmatrix} d(z). \tag{18}$$

As it was discussed earlier, the H_∞ controller ensures that the H_∞ norm of the CL system is less than some constant value, denoted γ.

$$\|g(z)\|_\infty < \gamma. \tag{19}$$

The upper bound achieved for $\|g(z)\|_\infty$ was $\gamma = 0.6415$. This value for γ is larger than the one obtained during the MIMO H_∞ design procedure, mainly because the effective influence function was not taken into consideration in the SISO model.

The resulting H_∞ controller achieves a disturbance rejection bandwidth for the SISO CL system of 80 z, while the peak of sensitivity TF remains below 10 B. Moreover, the sensitivity TF never crosses the -3 dB point, which suggests that the SISO H_∞ controller can achieve a CL bandwidth of 500 Hz.

All of the controller zeros as well as two of the poles are located close to the origin. The two remaining poles are located at $z = 1$ and $z = -9.0518e-01$. As it was done for the 56^{th} order controller, the order of the SISO H_∞ controller was reduced by applying model reduction to the full order controller. Thus, the fourth order H_∞ controller was reduced to a second order controller denoted as $k_\infty(z)$.

No loss of performance is detected since the disturbance rejection bandwidth remains at 80 Hz, while keeping the maximum peak of the Bode plot below 10 dB and the complementary sensitivity function never crosses the -3 dB point while its maximum value is below 0.5 dB.

Is noted that the model reduction has eliminated the two poles located closest to the origin while keeping unchanged the two remaining poles. On the other hand,

the zeros of the full order controller were all real and located close to the origin, while after the model reduction the two remaining zeros consist of non-zero real and imaginary parts located symmetrically about the real axis.

The next step was to extend the reduced order SISO design to a MIMO controller. Since the MIMO controller is not intended to affect the piston, waffle, tip and tilt modes, a 12×12 controller was first obtained. Based on our observations in Section 6, this 12×12 controller which will be denoted as $\overline{\boldsymbol{H}}(z)$, can be formed as the product of a diagonal compensator postmultiplied by a constant matrix. This constant matrix is the inverse of the adaptive optics open-loop dc gain matrix, when projected into the $\Re^{12}$ subspace orthogonal to piston, waffle, tip and tilt. Therefore, $\overline{\boldsymbol{H}}(z)$ is the following:

$$\overline{\boldsymbol{H}}(z) = k_\infty(z)(\boldsymbol{P}_r * \boldsymbol{G}_{\text{eff}}(1) * \boldsymbol{P}_r^T)^{-1}. \tag{20}$$

This controller should next be projected to the $\Re^{16}$ space before it can be applied to the adaptive optics system. Therefore, the extended controller is the following:

$$\boldsymbol{H}(z) = \boldsymbol{P}_r^T * \overline{\boldsymbol{H}}(z) * \boldsymbol{P}_r. \tag{21}$$

The resulting controller, when interconnected with the adaptive optics plant model, produced sensitivity and complementary sensitivity TF matrices whose SV Bode plots are shown in Figure 6 and Figure 7.

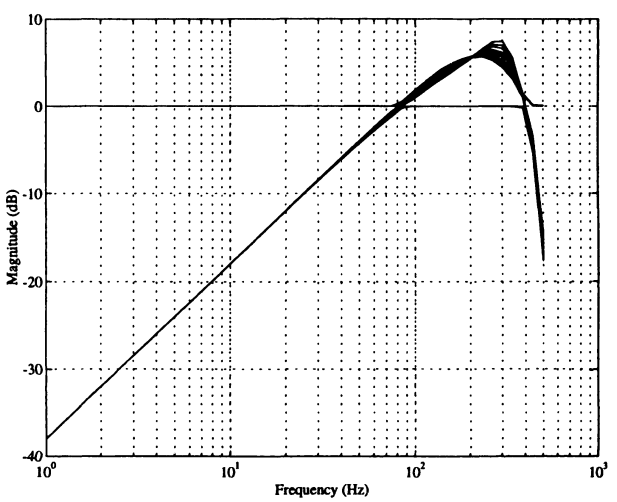

Fig. 6. Sensitivity TF with controller $\boldsymbol{H}(z)$.

Using $\boldsymbol{H}(z)$ as the controller a disturbance rejection bandwidth of 80 Hz is achieved, identical to the one when the reduced order H_∞ controller (24^{th} order) was applied. The H_∞ norm of the sensitivity has increased by 1 dB. However at low frequencies the spacing between the singular values has been reduced. This decrease of the singular value spacing implies that $\boldsymbol{H}(z)$, at frequencies below 200 Hz, achieves a

better diagonalization of the CL system than that achieved by the 24^{th} order H_∞ controller.

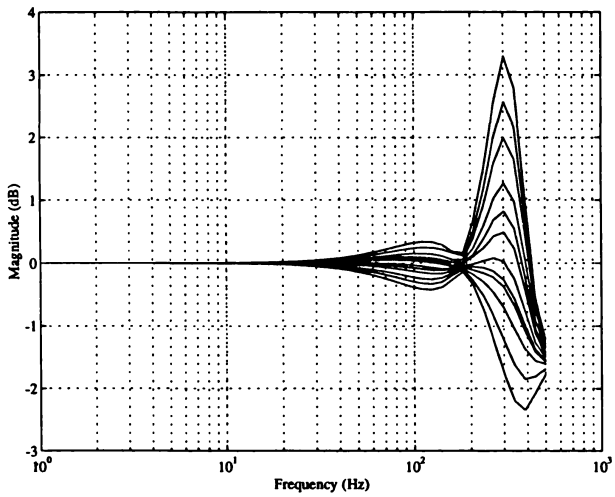

Fig. 7. Complementary sensitivity TF with controller $H(z)$.

The H_∞ norm of the complementary sensitivity function has increased from 0.5 dB to 3 dB. However, using $H(z)$ in the CL system the -3 dB point is never crossed which implies a CL bandwidth of 500 Hz. It should be also noted that the separation of the singular values of the complementary sensitivity TF at high frequencies has increased with this design when compared with the reduced order H_∞ controller. The results obtained by the SV Bode plots of the sensitivity and CL TFs presented above, are summarized in Table 1 where ω represents the closed-loop dominant resonant frequency.

Table 1. Summary of SV Bode plots.

H_∞ Contr.	CL BW	Dist. Reject. BW	$\|T\|_\infty$	$\|S\|_\infty$	ω
56^{th} Ord.	260 Hz	80 Hz	1 dB	6 dB	210 Hz
24^{th} Ord.	280 Hz	70 Hz	1 dB	6 dB	300 Hz
Approx.	500 Hz	80 Hz	4 dB	8 dB	310 Hz

8. CONCLUSIONS

In this paper we designed H_∞ controllers for an experimental adaptive optics system. A MIMO design methodology such as the H_∞ control design methodology is

necessary because of the loop coupling introduced by influence function spillovers and mode removal. The CL frequency domain performance characteristics of the H_∞ controller is superior to those of the PID-based controllers shown in a previous paper [8]. We then analyzed the structure of the reduced order H_∞ controller and developed a control design technique which requires only the synthesis of a SISO H_∞ controller followed by certain matrix multiplications. This has the potential for greatly simplifying control designs for realistic systems with hundreds (or thousands) of actuators.

(Received April 8, 1998.)

REFERENCES

[1] J. N. Aubrun, K. R. Lorell, T. S. Mast and J. E. Nelson: Dynamic analysis of the actively controlled segmented mirror of the W. M. Keck ten meter telescope. IEEE Control Systems Magazine, December 1987.
[2] H. W. Babcock: Adaptive optics revisited. Science *249* (1990), 253–257.
[3] C. Boyer: Adaptive optics for high resolution imagery: Control algorithms for optimized modal corrections. In: Proc. of the SPIE, Vol. 1780, 1992.
[4] J. D. Downie and J. W. Goodman: Optimal wavefront control for adaptive segmented mirrors. Appl. Optics *28* (1989), No. 4.
[5] B. L. Ellerbroek, C. Van Loan, N. Pitsianis and R. J. Plemmons: Optimizing closed loop adaptive optics performance using multiple control bandwidths. J. Opt. Soc. Amer. A *11* (1994).
[6] B. Francis: A Course in Control Theory. Springer–Verlag, Berlin 1987.
[7] J. Huang, D. P. Looze, N. Denis and D. A. Castañon: Dynamic modeling and identification of an adaptive optics system. In: Proc. 4th IEEE Conf. on Control Applications, Albany 1995.
[8] J. Huang, D. P. Looze, N. Denis and D. A. Castañon: Control designs for an adaptive optics system. In: 34th IEEE Conference on Decision and Control Proceedings, New Orleans 1995.
[9] B. C. Moore: Principal components analysis in linear systems: controllability, observability, and model reduction. IEEE Trans. Automat. Control *AC-26* (1981), No. 2.
[10] Special Issue on Adaptive Optics. Lincoln Laboratory J. *5* (1992), No. 1.
[11] A. Tebo: Adaptive Optics. OE Reports, No. 96, 1991.
[12] R. K. Tyson: Principles of Adaptive Optics. Academic Press, San Diego 1991.

Nikolaos Denis, Alphatech, Inc., Burlington, MA 01803. U. S. A.
e-mail: denis@alphatech.com

Douglas Looze, University of Massachusetts, Amherst, MA 01003. U. S. A.
e-mail: looze@ecs.umass.edu

Jim Huang, Raytheon, NH. U. S. A.
e-mail: jim.huang@res.raytheon.com

David Castañon, Boston University, Boston, MA. U. S. A.
e-mail: castanon@alphatech.con